Supplementary materials for

2D Zn/ZnO via the Solid-Liquid Interfacial Engineering for Room Temperature Optoelectronic Gas Sensing

Xiao Long Cao[1], Zhong Li[1, 2 *], Kai Yu Yao[1], Fei Yue Wu[1], Bo Xin Hu[1], Tao Tang[1 *], Yin Fen Cheng[3], Yi Liang[1], Jing Hao Zhuang[1], Xin Yi Hu[1], Qi Zhang[1], Nianzhong Ma[1], Yao Yang Liu[1], Qing Wen Song[1], Qian Wang[4], Dazhi Chen[1], and Jian Zhen Ou[1, 5] *

[1]Key Laboratory of Advanced Technologies of Materials, Ministry of Education, School of Materials Science and Engineering, Southwest Jiaotong University, Chengdu 610031, China

[2]Jiangsu Key Laboratory of Advanced Structural Materials and Application Technology, Nanjing Institute of Technology, Nanjing 211167, China

[3]Institute of Advanced Study, Chengdu University, Chengdu 610106, China

[4]School of Material Science and Engineering, Lanzhou Jiaotong University, Lanzhou 730070, PR China.

[5]School of Engineering, RMIT University, Melbourne, Victoria 3000, Australia

*Corresponding author. E-mail: zhong.li@swjtu.edu.cn (Z. Li), tangtao@my.swjtu.edu.cn (T Tang), jzou@swjtu.edu.cn, jianzhen.ou@rmit.edu.au (J. Z. Ou)

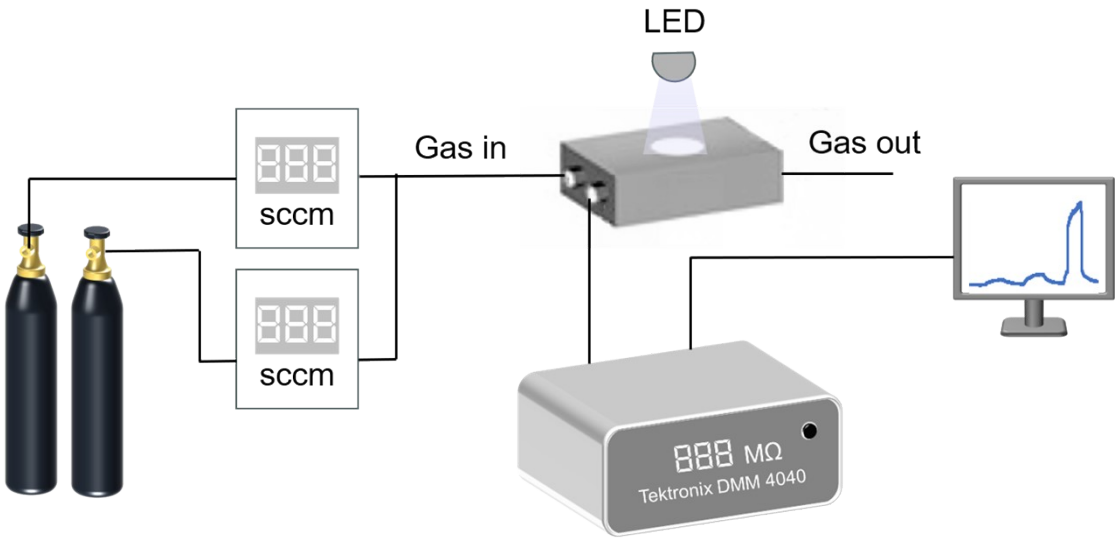

Fig. S1 Schematic of the set-up used for gas sensing tests.

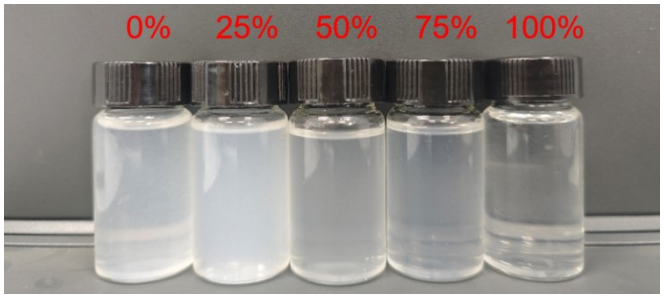

Fig. S2 The photograph of Zn/ZnO heterostructure suspension obtained in the mixed solution containing 0, 25, 50, 75, 100%v/v ethanol.

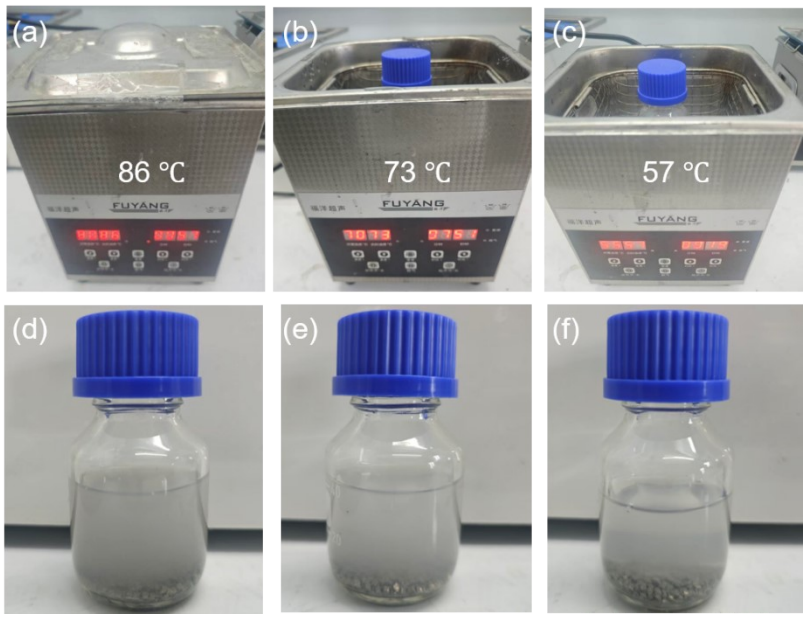

Fig. S3 a)-c) The ultrasonic temperature control at 86 ℃, 73 ℃, and 57 ℃ is achieved

by closing the cover of the ultrasound machine and turning on heating at the same time, opening the cover of the ultrasound machine and turning on heating, and just opening the lid of the ultrasound machine, respectively. d)-f) The dispersion of Zn/ZnO obtained from sonicated Zn particles at 86 ℃, 73 ℃, and 57 ℃, respectively.

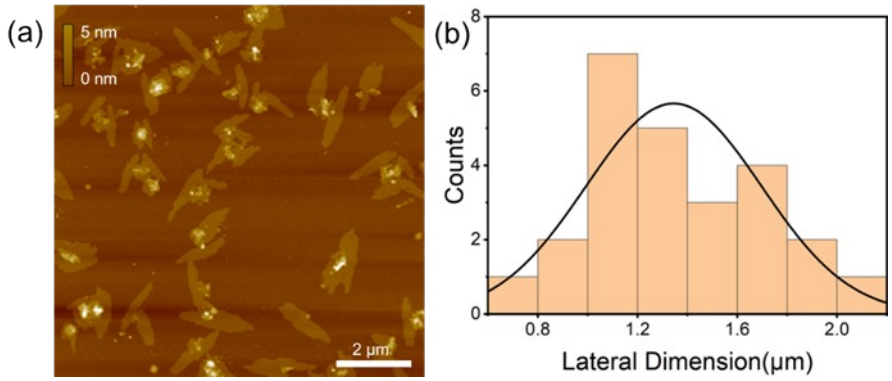

Fig. S4 The statistical analysis of the lateral dimension of ZnO nanosheets.

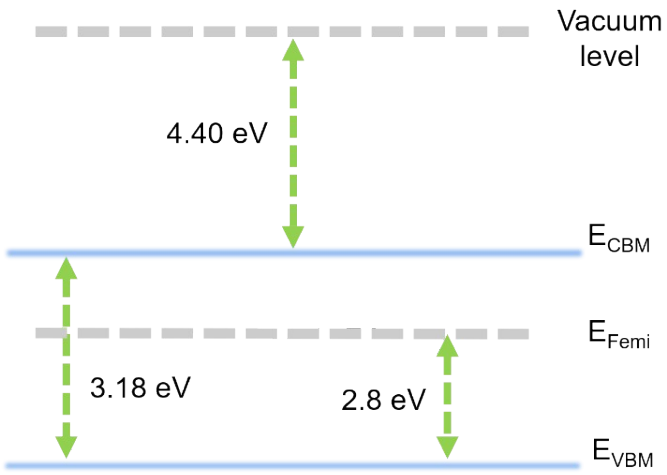

Fig. S5 The energy band diagram of Zn/ZnO heterostructure.

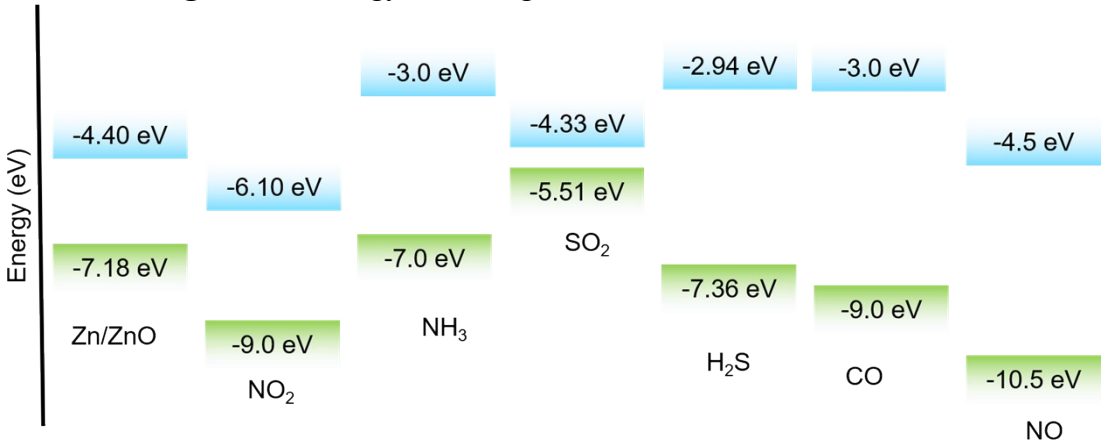

Fig.S6 Energy band diagram of 2D Zn/ZnO, NO_2, NH_3, SO_2, H_2S, CO and NO

molecule.

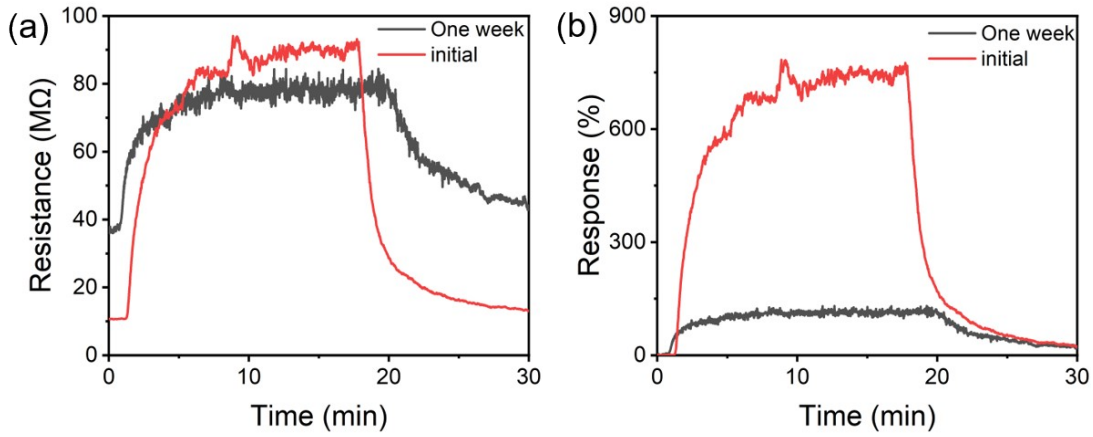

Fig. S7 Long-term stability of the Zn/ZnO heterostructure sensor to 10 ppm NO_2 at room temperature and purple light. (a) The resistance curves and (b) corresponding response curves.

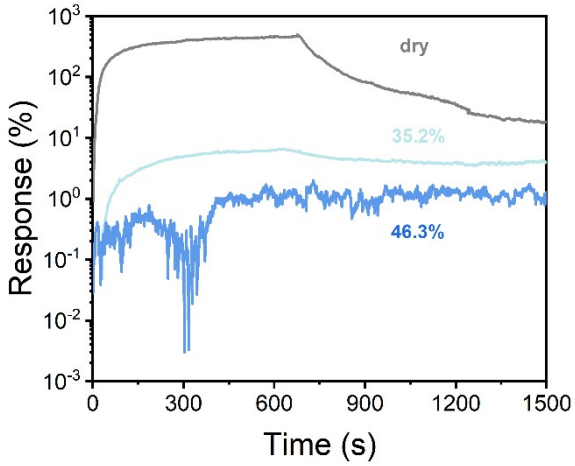

Fig. S8 The logarithmic plot of gas response of the Zn/ZnO heterostructure sensor to 5 ppm NO_2 at room temperature, purple light irradiation and different humidity level.

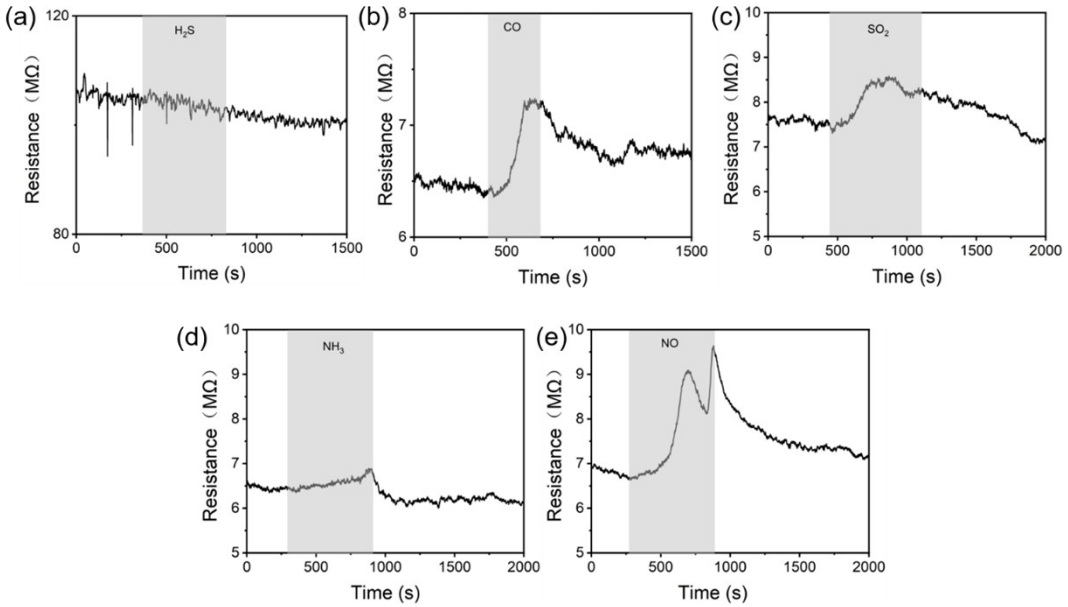

Fig. S9 Resistance transient of Zn/ZnO heterostructure based sensor under (a) 50 ppm H_2S, (b) 500 ppm CO, (c) 50 ppm SO_2, (d) 300 ppm NH_3 and (e) 10 ppm NO.

Table S1 The sensing performance comparison of Zn/ZnO heterostructure based sensor towards 10 ppm NO_2 under the different light irradiation.

Light source	Wavelength (nm)	Baseline resistance (MΩ)	Response (%)	Recovery time (min)
UV	365	4	293.3	5.23
Purple	405	10	705.3	5.79
Blue	450	560	29.1	6.85
No light	-	Overload	-	-

Table S2 Ppb-level NO_2 gas sensing performance of different gas sensors.

Materials	Conc. (ppb)	Temp. (℃)	Res.	Synthesis method	Sensor device fabrication	Comments
Co-SnS_2[1]	1	190	89.7%	Hydrothermal	Electrode deposition	High work temperature
ZnO/$Ti_3C_2T_x$[2]	500	180	46.3%	Solvothermal + Etching	Drop-casting	
MoO_3[3]	50	100	2.3%	Dual-zone finance	Electrode deposition	
In_2O_3[4]	50	92	40%	Biomass-templated calcination	Drop-casting	
MoS_2[5]	2.5	RT	1120%	Mechanical exfoliation	Electrode deposition	Complex device preparation

				+ Etching		
MoS_2[6]	120	RT	~40%	CVD		
SnS_2/MWCNT[7]	25	20	3%	Hydrothermal	Drop-casting	Long material synthesis time
Zn/ZnO (This work)	50	RT	14.5%	Solid-liquid reaction		Short material synthesis time; Simple device preparation; RT work

Reference

1. J. N. Chang, C. Qin, Y. Zhang, L. H. Zhu, Y. Zhang, Y. Wang and J. L. Cao, Abundant active sites triggered by Co-doped SnS_2 for ppb-level NO_2 detection, Sens. Actuator B-Chem., 2023, 395, 11.
2. L. Chen, X. Chen, F. Wang, Y. Tong, K. W. Zhang, Z. B. Han and M. Z. Zhang, MOF-derived ZnO/$Ti_3C_2T_x$ MXene heterostructures for ultrafast ppb-level detection of H_2 and NO_2 gases, Sens. Actuator B-Chem., 2026, 447, 10.
3. W. Li, Q. D. Ou, X. D. Wang, K. J. Xing, T. Tesfamichael, N. Motta and D. C. Qi, Large-sized α-MoO_3 layered single crystals for superior NO_2 gas sensing, Applied Surface Science, 2022, 586, 12.
4. N. Wang, J. X. Ye, J. B. Sun, X. F. Zhang, Z. P. Deng, Y. M. Xu, L. H. Huo and S. Gao, Rapid and accurate detection of highly toxic NO_2 gas based on catkins biomass-derived porous In_2O_3 microtubes at low temperature, Sens. Actuator B-Chem., 2022, 361, 10.
5. A. V. Agrawal, A. Y. Polyakov, J. Eriksson, T. J. Antosiewicz and T. O. Shegai, Humidity-Enhanced NO_2 Gas Sensing Using Atomically Sharp Edges in Multilayer MoS_2, Small Struct., 2025, 6, 15.
6. B. Cho, A. R. Kim, Y. Park, J. Yoon, Y. J. Lee, S. Lee, T. J. Yoo, C. G. Kang, B. H. Lee, H. C. Ko, D. H. Kim and M. G. Hahm, Bifunctional Sensing Characteristics of Chemical Vapor Deposition Synthesized Atomic-Layered MoS_2, ACS Appl. Mater. Interfaces, 2015, 7, 2952-2959.
7. I. S. Saggu, S. Singh, K. W. Chen, Z. X. Xuan, M. T. Swihart and S. Sharma, Ultrasensitive Room-Temperature NO_2 Detection Using SnS_2/MWCNT Composites and Accelerated Recovery Kinetics by UV Activation, ACS Sens., 2023.